PHYSICAL REVIEW D **85,** 034020 (2012)

Next-to-leading order QCD effect of W' on top quark forward-backward asymmetry

Kai Yan,[1] Jian Wang,[1] Ding Yu Shao,[1] and Chong Sheng Li[1,2,*]

[1]*Department of Physics and State Key Laboratory of Nuclear Physics and Technology, Peking University, Beijing 100871, China*
[2]*Center for High Energy Physics, Peking University, Beijing 100871, China*

(Received 30 October 2011; published 10 February 2012)

We present the calculations of the complete next-to-leading order QCD corrections to the total cross section, invariant mass distribution, and the forward-backward asymmetry ($A_{\rm FB}$) of top quark pair production mediated by the W' boson. Our results show that in the best fit point in the parameter space allowed by data at the Tevatron, the next-to-leading order corrections change the new physics contributions to the total cross section slightly, but increase the $A_{\rm FB}$ in the large invariant mass region by about 9%. Moreover, we evaluate the total cross section and charge asymmetry (A_C) of top pair production at the LHC, and find that both total cross section and A_C can be used to distinguish new physics from the standard model with the integrated luminosity increasing.

DOI: 10.1103/PhysRevD.85.034020 PACS numbers: 14.65.Ha, 12.38.Bx, 12.60.−i

I. INTRODUCTION

The top quark is the heaviest particle discovered so far, with a mass close to the electroweak symmetry breaking scale. Thus it is a wonderful probe for the electroweak breaking mechanism and new physics (NP) beyond the standard model (SM) through its productions and decays at colliders. The forward-backward asymmetry ($A_{\rm FB}$) of the top quark pair production is one of the interesting observables in the top quark sector. Within the SM, $A_{\rm FB}$ is absent at the tree level in QCD due to charge symmetry, and occurs at QCD next-to-leading order (NLO) with the prediction $A_{\rm FB} \sim 6\%$ in the $t\bar{t}$ rest frame [1–6]. In the last few years, the D0 and CDF Collaborations have measured $A_{\rm FB}$ at the Tevatron [7–10]. Recently, the CDF Collaborations announced that, for the invariant mass of the top quark pair $m_{t\bar{t}} \geq 450$ GeV, the measured asymmetry in the $t\bar{t}$ rest frame is $A_{\rm FB} = 0.475 \pm 0.114$ [9], which differs by 3.4σ from the SM predictions $A_{\rm FB} = 0.088 \pm 0.013$. This deviation has stimulated a number of theoretical papers on NP models, such as new gauge bosons and axigluons [11–81].

Recent studies are concerned with the problem of top asymmetry by a flavor-changing interaction mediated by a charged vector boson, W' [13,82], which can be described by the following effective Lagrangian [13]:

$$\mathcal{L}_{\rm NP} = -g' W'^{-}_{\mu} \bar{d} \gamma^{\mu} (f_L P_L + f_R P_R) t + \text{H.c.}, \quad (1)$$

where $P_{R,L} = (1 \pm \gamma^5)/2$ are the chirality projection operators, $f_{L,R}$ are the chiral couplings of the W' boson with fermions, satisfying $f_L^2 + f_R^2 = 1$, and g' is the coupling constant. The study of this model at the leading order (LO) has been explored in Refs. [22,32]. It is shown that, for suitable parameters, this model can explain the $A_{\rm FB}$ observed at the Tevatron within 1–1.5σ of the data. It is well known that the LO cross sections for process at the hadron colliders suffer from large uncertainties due to the arbitrary choice of the renormalization and factorization scales, thus it is necessary to include higher order corrections to make a reliable theoretical prediction. Besides, at the NLO level, virtual corrections, real gluon emission, and massless (anti) quark emission can lead to a sizable difference between the differential top and antitop production process [1,2], which will also contribute to $A_{\rm FB}$. Therefore it is necessary to perform complete calculations of NLO contributions in the W' model.

There is a similar work in the Z' model [83], where the NLO QCD corrections up to $\mathcal{O}(\alpha_s^2 g'^2)$ are taken into account. In this work, we calculate both $\mathcal{O}(\alpha_s^2 g'^2)$ and $\mathcal{O}(\alpha_s g'^4)$ NP contributions, and the latter term is definitely not smaller than the former so that it should not be neglected. Based on the above calculation, we fit the data at the Tevatron, including total cross section, the invariant mass distribution, and the $A_{\rm FB}$, and find the allowed parameter space. Moreover, we study the top quark pair production at the Large Hadron Collider (LHC) induced by a W' boson at the NLO QCD level. Since the gluon fusion channel dominates in the $t\bar{t}$ production process at the LHC, it is difficult to probe NP effects on $A_{\rm FB}$ from early LHC results. However, LHC will be able to detect the potential NP effect on the charge asymmetry (A_C) when the integrated luminosity increases in the future.

The arrangement of this paper is as follows. In Sec. II we show the LO results of top quark pair production. In Sec. III, we present the details of the NLO calculations, including the virtual and real corrections. In Sec. IV we show the numerical results. The conclusion is given in Sec. V.

II. LEADING ORDER RESULTS

Up to NLO, the $t\bar{t}$ production amplitudes, including NP contributions, can be written as

$$\mathcal{M}^{t\bar{t}} = \alpha_s f_{\rm SM}^{\rm LO} + g'^2 f_{\rm NP}^{\rm LO} + \alpha_s^2 f_{\rm SM}^{\rm NLO} + \alpha_s g'^2 f_{\rm NP}^{\rm NLO}. \quad (2)$$

*csli@pku.edu.cn

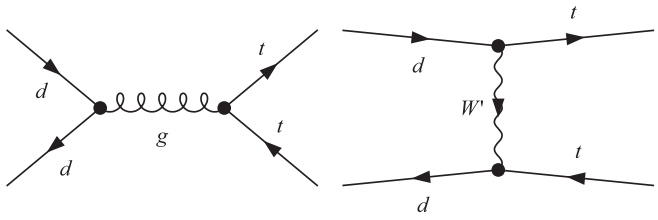

FIG. 1. LO Feynman diagrams for $d\bar{d} \to t\bar{t}$.

And the $t\bar{t}$ amplitude squared is

$$\begin{aligned}|\mathcal{M}^{t\bar{t}}|^2 = {} & \alpha_s^2 f_{\mathrm{SM}}^{\mathrm{LO}} f_{\mathrm{SM}}^{\mathrm{LO}^*} + 2\alpha_s g'^2 \,\mathrm{Re}(f_{\mathrm{SM}}^{\mathrm{LO}} f_{\mathrm{NP}}^{\mathrm{LO}^*}) \\ & + g'^4 f_{\mathrm{NP}}^{\mathrm{LO}} f_{\mathrm{NP}}^{\mathrm{LO}^*} + 2\alpha_s^3 \,\mathrm{Re}(f_{\mathrm{SM}}^{\mathrm{LO}} f_{\mathrm{SM}}^{\mathrm{NLO}^*}) \\ & + 2\alpha_s^2 g'^2 [\mathrm{Re}(f_{\mathrm{SM}}^{\mathrm{LO}} f_{\mathrm{NP}}^{\mathrm{NLO}^*}) + \mathrm{Re}(f_{\mathrm{NP}}^{\mathrm{LO}} f_{\mathrm{SM}}^{\mathrm{NLO}^*})] \\ & + 2\alpha_s g'^4 \,\mathrm{Re}(f_{\mathrm{NP}}^{\mathrm{LO}} f_{\mathrm{NP}}^{\mathrm{NLO}^*}). \end{aligned} \tag{3}$$

The first three terms are the LO results of the SM and NP. The fourth term is the SM NLO result, and the fifth term is the interference contribution. The NP NLO result is given by the last term.

The LO Feynman diagrams for the subprocess $d(p_1)\bar{d}(p_2) \to t(p_3)\bar{t}(p_4)$ induced by the NP and the SM QCD interactions are shown in Fig. 1, and the LO partonic cross section can be written as

$$\hat{\sigma}^{\mathrm{LO}} = \hat{\sigma}_{\mathrm{SM}}^{\mathrm{LO}} + \hat{\sigma}_{\mathrm{INT}}^{\mathrm{LO}} + \hat{\sigma}_{\mathrm{NPS}}^{\mathrm{LO}}, \tag{4}$$

where subscripts SM, INT, and NPS denote the SM channel contributions, the interference between SM and NP channels, and NP channel contributions, respectively. The LO partonic differential cross sections are given by

$$\frac{d\hat{\sigma}_{\mathrm{SM}}^{\mathrm{LO}}}{d\cos\theta} = \frac{2\pi\beta}{9\hat{s}} \frac{\alpha_s^2}{\hat{s}^2} [6m_t^4 - 4m_t^2(t+u) + t^2 + u^2], \tag{5}$$

$$\begin{aligned}\frac{d\hat{\sigma}_{\mathrm{INT}}^{\mathrm{LO}}}{d\cos\theta} = {} & \frac{2\beta}{9\hat{s}} \frac{\alpha_s g'^2}{m_{W'}^2 s(m_{W'}^2 - t)} (f_R^2 + f_L^2) \\ & \times [3m_t^6 + m_t^4(6m_{W'}^2 - 3t - u) \\ & + m_t^2(t^2 - 2m_{W'}^2(t+3u)) + 2m_{W'}^2 u^2], \end{aligned} \tag{6}$$

$$\begin{aligned}\frac{d\hat{\sigma}_{\mathrm{NPS}}^{\mathrm{LO}}}{d\cos\theta} = {} & \frac{\beta}{8\pi\hat{s}} \frac{g'^4}{m_{W'}^4 (m_{W'}^2 - t)^2} \{(f_R^4 + f_L^4) \\ & \times [m_t^8 - 2m_t^6 t + m_t^4(4m_{W'}^4 + 4m_{W'}^2 s + t^2) \\ & - 8m_t^2 m_{W'}^4 u + 4m_{W'}^4 u^2] + 2f_R^2 f_L^2 [m_t^8 - 2m_t^6 t \\ & + m_t^4(4m_{W'}^2 s + t^2) - 8m_{W'}^2 m_{W'}^4 s + 4m_{W'}^4 s^2]\}, \end{aligned} \tag{7}$$

where the Mandelstam variables s, t, and u are defined as follows:

$$s = (p_1 + p_2)^2, \quad t = (p_1 - p_3)^2, \quad u = (p_1 - p_4)^2. \tag{8}$$

The relations between them are

$$\begin{aligned} m_t^2 - t &= s(1 - \beta\cos\theta)/2, \\ m_t^2 - u &= s(1 + \beta\cos\theta)/2, \end{aligned} \tag{9}$$

where $\beta = \sqrt{1 - 4m_t^2/s}$, and θ is the polar angle of the outgoing top quark in the $t\bar{t}$ rest frame. The colors and spins of the incoming (outgoing) particles have been averaged (summed) over. Integrating over $\cos\theta$, we obtain the LO result of $d\bar{d} \to t\bar{t}$ partonic cross section.

The LO total cross section at the hadron collider is obtained by convoluting the partonic cross section with the parton distribution functions (PDFs) $G_{i/A(B)}$ for the initial hadrons A and B:

$$\sigma^{\mathrm{LO}} = \sum_{a,b} \int_\tau^1 dx_a \int_{\tau/x_a}^1 dx_b G_{a/A}(x_a, \mu_f) G_{b/B}(x_b, \mu_f) \hat{\sigma}^{\mathrm{LO}}, \tag{10}$$

where $\tau = 4m_t^2/s$.

III. NEXT-TO-LEADING ORDER QCD CORRECTIONS

The NLO corrections to the top quark pair production consist of the virtual corrections, generated by loop diagrams of colored particles, and the real corrections with the radiation of a real gluon or a massless (anti)quark. For the real corrections, we used the two cutoff phase space slicing method to subtract the infrared (IR) divergences [84].

A. Virtual corrections

The virtual corrections for the top quark pair production include the box diagrams, triangle diagrams, and self-energy diagrams induced by SM QCD and NP interactions as shown in Figs. 2 and 3, respectively. The renormalized virtual amplitudes are given as follows:

$$\begin{aligned}\mathcal{M}_{\mathrm{SM}}^{\mathrm{ren}} = {} & \frac{\alpha_s}{4\pi} C_\epsilon C_F \left(\frac{2}{\epsilon_{\mathrm{UV}}}\right) \mathcal{M}_{\mathrm{SM}}^{\mathrm{LO}} + (\delta Z_2^q + \delta Z_2^t \\ & + 2\delta g_s) \mathcal{M}_{\mathrm{SM}}^{\mathrm{LO}} + \mathcal{M}_{\mathrm{SM}}^{\mathrm{fin}}, \end{aligned} \tag{11}$$

$$\begin{aligned}\mathcal{M}_{\mathrm{NP}}^{\mathrm{ren}} = {} & \frac{\alpha_s}{4\pi} C_\epsilon C_F \left(\frac{2}{\epsilon_{\mathrm{UV}}}\right) \mathcal{M}_{\mathrm{NP}}^{\mathrm{LO}} + (\delta Z_2^q + \delta Z_2^t) \\ & \times \mathcal{M}_{\mathrm{NP}}^{\mathrm{LO}} + \mathcal{M}_{\mathrm{NP}}^{\mathrm{fin}}, \end{aligned} \tag{12}$$

where $C_\epsilon = (4\pi)^\epsilon \frac{1}{\Gamma(1-\varepsilon)}$. $\mathcal{M}_{\mathrm{SM}}^{\mathrm{fin}}$ and $\mathcal{M}_{\mathrm{NP}}^{\mathrm{fin}}$ are ultraviolet (UV) finite terms for SM and NP processes. All the UV divergences in the loop diagrams are canceled by counterterms δZ_2^q for the wave functions of the external fields in the on-shell scheme, and δg_s for the strong coupling constant in the $\overline{\mathrm{MS}}$ scheme modified to decouple the top quark [85],

$$\delta Z_2^q = -\frac{\alpha_s}{3\pi} C_\epsilon \left(\frac{1}{\epsilon_{\mathrm{UV}}} - \frac{1}{\epsilon_{\mathrm{IR}}}\right), \tag{13}$$

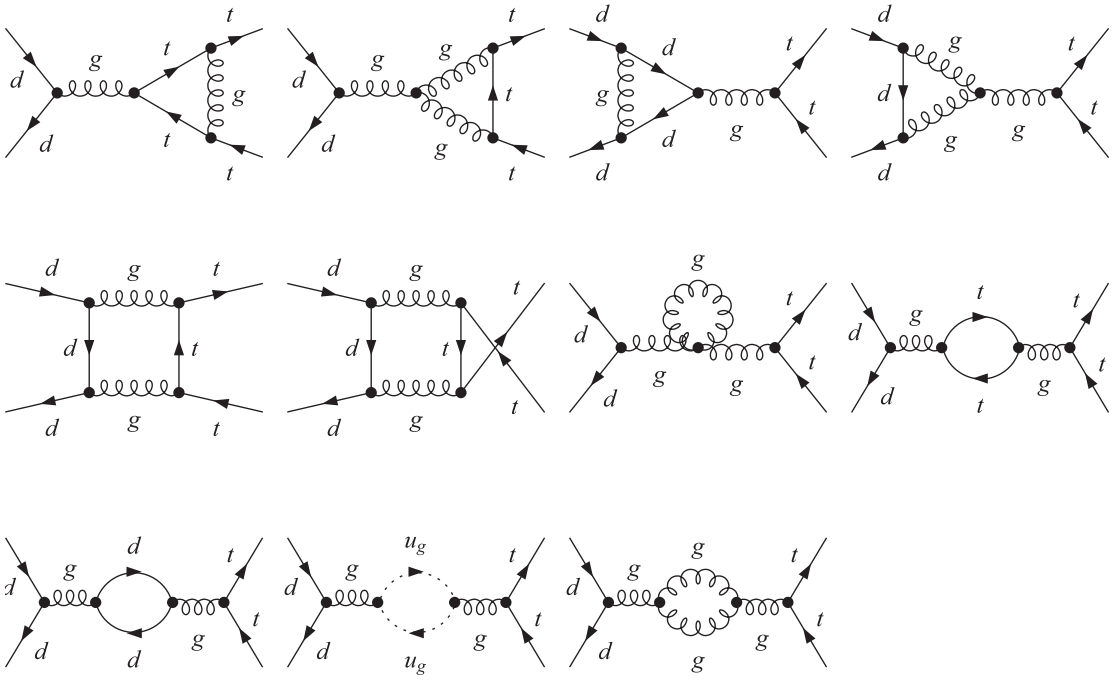

FIG. 2. One-loop virtual Feynman diagrams for $d\bar{d} \to t\bar{t}$ induced by SM QCD interactions.

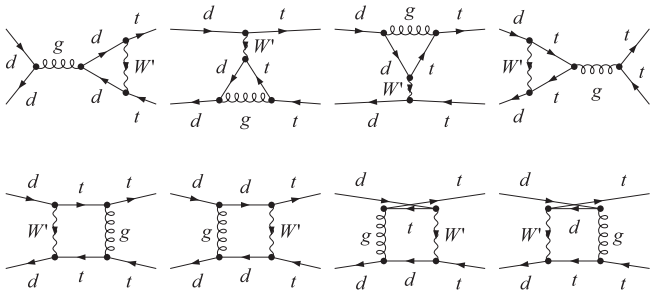

FIG. 3. One-loop virtual Feynman diagrams for $d\bar{d} \to t\bar{t}$ induced by NP interactions.

$$\delta Z_2^t = -\frac{\alpha_s}{3\pi} C_\epsilon \left(\frac{1}{\epsilon_{\rm UV}} + \frac{2}{\epsilon_{\rm IR}} + 4 + 3 \ln \frac{\mu_r^2}{m_t^2} \right), \tag{14}$$

$$\delta g_s = \frac{\alpha_s}{4\pi} C_\epsilon \left(\frac{n_f}{3} - \frac{11}{2} \right) + \frac{\alpha_s}{12\pi} C_\epsilon \left(\frac{1}{\epsilon_{\rm UV}} + \ln \frac{\mu_r^2}{m_t^2} \right), \tag{15}$$

where $n_f = 5$ and μ_r is the renormalization scale. The renormalized amplitudes $\mathcal{M}_{\rm SM}^{\rm ren}$ and $\mathcal{M}_{\rm NP}^{\rm ren}$ are UV finite, but still contain IR divergences. The virtual corrections for subprocess $q\bar{q} \to t\bar{t}$ can be expressed as

$$\begin{aligned} d\hat{\sigma}^{\rm virt} &= d\hat{\sigma}_{\rm SM}^{\rm virt} + d\hat{\sigma}_{\rm NPS}^{\rm virt} + d\hat{\sigma}_{\rm INT}^{\rm virt} \\ &= \frac{1}{2s} d\Gamma_2 \{ 2\,{\rm Re}(\mathcal{M}_{\rm SM}^{\rm ren} \mathcal{M}_{\rm SM}^{\rm LO*}) + 2\,{\rm Re}(\mathcal{M}_{\rm NP}^{\rm ren} \mathcal{M}_{\rm NP}^{\rm LO*}) \\ &\quad + 2\,{\rm Re}(\mathcal{M}_{\rm SM}^{\rm ren} \mathcal{M}_{\rm NP}^{\rm LO*} + \mathcal{M}_{\rm NP}^{\rm ren} \mathcal{M}_{\rm SM}^{\rm LO*}) \}. \end{aligned} \tag{16}$$

We have calculated the SM contribution and find the result agrees with that in Ref. [86]. The one-loop correction for the cross section induced by NP interactions, with IR singularities separated from finite terms, is given by

$$d\hat{\sigma}^{\rm virt} = \frac{\alpha_s}{2\pi} C_\epsilon \left[\frac{(A_2^v)_{\rm INT}}{\epsilon_{\rm IR}^2} + \frac{(A_1^v)_{\rm INT}}{\epsilon_{\rm IR}} \right] d\hat{\sigma}_{\rm INT}^{\rm LO} \tag{17}$$

$$+ \frac{\alpha_s}{2\pi} C_\epsilon \left[\frac{(A_2^v)_{\rm NPS}}{\epsilon_{\rm IR}^2} + \frac{(A_1^v)_{\rm NPS}}{\epsilon_{\rm IR}} \right] d\hat{\sigma}_{\rm NPS}^{\rm LO} + d\hat{\sigma}^{\rm virt,fin}, \tag{18}$$

where

$$(A_2^v)_{\rm INT} = -2C_F, \tag{19}$$

$$(A_1^v)_{\rm INT} = \frac{C_F}{4} \left[16 \ln \frac{-t_1}{\mu_r^2} + 2 \ln \frac{-u_1}{\mu_r^2} + 9 \ln \frac{\mu_r^2}{m_t^2} + \ln \frac{\mu_r^2}{s} - \frac{1+\beta^2}{2\beta} \ln \frac{\beta+1}{1-\beta} - 20 \right], \tag{20}$$

and

$$(A_2^v)_{\rm NPS} = -2C_F, \tag{21}$$

$$(A_1^v)_{\rm NPS} = 2C_F \left[2 \ln \frac{-t_1}{\mu_r^2} + \ln \frac{\mu_r^2}{m_t^2} - \frac{5}{2} \right], \tag{22}$$

with $t_1 = t - m_t^2$, and $u_1 = u - m_t^2$. The IR divergent terms are proportional to the LO partonic cross sections $\hat{\sigma}_{\rm INT}^{\rm LO}$ and $\hat{\sigma}_{\rm NPS}^{\rm LO}$. $\sigma^{\rm virt,fin}$ is the finite term of the virtual cross section.

B. Real corrections

At the NLO level the real corrections consist of the radiations of an additional gluon or massless (anti)quark in the final states as shown in Figs. 4 and 5.

The phase space integration for the real gluon emission will produce soft and collinear singularities, which can be isolated by slicing the phase space into different regions using suitable cutoffs. In this paper, we use the two cutoff phase space slicing method [84], which introduces two arbitrary small cutoff parameters, i.e. soft cutoff parameters δ_s and collinear parameters δ_c, to decompose the three-body phase space into three regions.

First, the phase space is separated into two regions by the soft cutoff parameters δ_s, according to whether the energy of the emitted gluon is soft, i.e. $E_5 \leq \delta_s\sqrt{s_{12}}/2$, or hard, i.e. $E_5 > \delta_s\sqrt{s_{12}}/2$. Then the collinear cutoff parameter δ_c is introduced to divide the hard gluon phase space into two regions, according to whether the Mandelstam variables $t_{i5} \equiv (p_i - p_5)^2$ $(i = 1, 2)$ satisfy the collinear condition $|t_{i5}| < \delta_c s_{12}$ or not. Thus we have

$$d\hat{\sigma}^{\rm Real} = d\hat{\sigma}^{S} + d\hat{\sigma}^{HC} + d\hat{\sigma}^{H\bar{C}}. \tag{23}$$

The hard noncollinear term $d\hat{\sigma}^{H\bar{C}}$ can be written as

$$d\hat{\sigma}^{H\bar{C}} = \frac{1}{2s_{12}}\int |\mathcal{M}_3|^2 d\Gamma_3|_{H\bar{C}} \tag{24}$$

which can be evaluated numerically using standard Monte Carlo techniques [87]. In the following sections, we discuss the parts containing the soft and hard collinear singularities.

In the limit that the energy of the emitted gluon becomes small, i.e. $E_5 \leq \delta_s\sqrt{s_{12}}/2$, the three-body cross section $d\hat{\sigma}^{S}$ can be factorized as

$$d\hat{\sigma}^{S} = \left[\frac{\alpha_s}{2\pi}C'_\epsilon\right]\sum_{i,j=1}^{4}\left(d\hat{\sigma}^{\rm LO}_{\rm INT}\frac{\mathcal{C}^{\rm INT}_{ij}}{\mathcal{C}^{\rm INT}_{0}} + d\hat{\sigma}^{\rm LO}_{\rm NPS}\frac{\mathcal{C}^{\rm NPS}_{ij}}{\mathcal{C}^{\rm NPS}_{0}}\right) \times \int dS\frac{-p_i\cdot p_j}{(p_i\cdot p_5)(p_j\cdot p_5)}, \tag{25}$$

where

$$C'_\epsilon = \frac{\Gamma(1-\epsilon)}{\Gamma(1-2\epsilon)}\left(\frac{4\pi\mu_r^2}{s_{12}}\right)^{\epsilon}.$$

The color charge factors $\mathcal{C}_{ij}$ are

$$\begin{aligned}&\mathcal{C}^{\rm INT}_{12} = \mathcal{C}^{\rm INT}_{34} = C_F/2, \qquad \mathcal{C}^{\rm INT}_{33} = \mathcal{C}^{\rm INT}_{44} = C_A C_F^2,\\ &\mathcal{C}^{\rm INT}_{13} = \mathcal{C}^{\rm INT}_{24} = -C_A C_F^2, \qquad \mathcal{C}^{\rm INT}_{14} = \mathcal{C}^{\rm INT}_{23} = -C_F/2,\\ &\mathcal{C}^{\rm INT}_{11} = \mathcal{C}^{\rm INT}_{22} = 0,\end{aligned} \tag{26}$$

and

$$\begin{aligned}&\mathcal{C}^{\rm NPS}_{13} = \mathcal{C}^{\rm NPS}_{24} = 3C_A C_F, \qquad \mathcal{C}^{\rm NPS}_{33} = \mathcal{C}^{\rm NPS}_{44} = -3C_A C_F,\\ &\mathcal{C}^{\rm NPS}_{11} = \mathcal{C}^{\rm NPS}_{22} = 0, \qquad \mathcal{C}^{\rm NPS}_{12} = \mathcal{C}^{\rm NPS}_{34} = \mathcal{C}^{\rm NPS}_{14} = \mathcal{C}^{\rm NPS}_{23} = 0.\end{aligned} \tag{27}$$

Here $\mathcal{C}^{\rm INT}_0 = C_A C_F$ and $\mathcal{C}^{\rm NPS}_0 = 9$ are the color factors of LO diagrams in Fig. 1.

The integration over the soft phase space is given by [84]

$$\int dS = \frac{1}{\pi}\left(\frac{4}{s_{12}}\right)^{-\epsilon}\int_0^{\delta_s\sqrt{s_{12}}/2} dE_5 E_5^{1-2\epsilon}\sin^{1-2\epsilon}\theta_1 d\theta_1 \times \sin^{-2\epsilon}\theta_2 d\theta_2. \tag{28}$$

We define

$$\mathcal{I}_{ij} = \int dS\frac{1}{(p_i\cdot p_5)(p_j\cdot p_5)}. \tag{29}$$

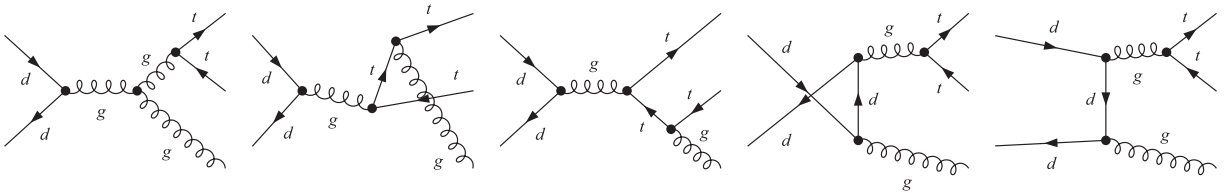

FIG. 4. Feynman diagrams for a gluon emission induced by SM QCD interactions. The diagrams for a (anti)quark emission can be obtained by crossing the initial-state (anti)quark with the final-state gluon.

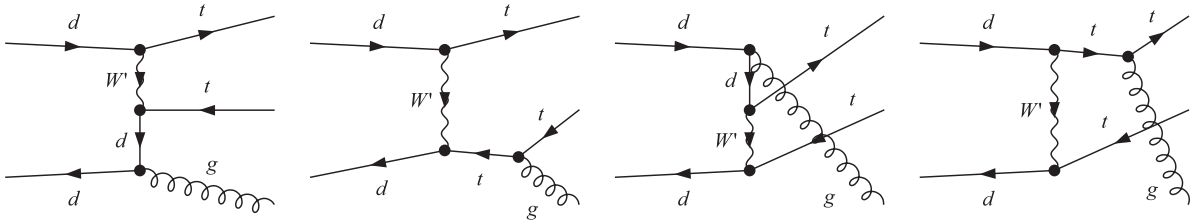

FIG. 5. Feynman diagrams for a gluon emission induced by NP interactions. The diagrams for a (anti)quark emission can be obtained by crossing the initial-state (anti)quark with the final-state gluon.

Then we have

$$\begin{aligned}
&\mathcal{I}_{11} = \mathcal{I}_{22} = 0,\\
&\mathcal{I}_{33} = \mathcal{I}_{44} = -\frac{1}{m_t^2}\frac{1}{\epsilon_{\rm IR}} + \mathcal{I}_{33}^{\rm fin},\\
&\mathcal{I}_{34} = \frac{2}{s}\left(-\frac{1}{\epsilon_{\rm IR}}\frac{1}{\beta}\ln\frac{\beta+1}{1-\beta}\right) + \mathcal{I}_{34}^{\rm fin},\\
&\mathcal{I}_{12} = \frac{2}{s}\left\{\frac{1}{\epsilon_{\rm IR}^2} + \frac{1}{\epsilon_{\rm IR}}(-2\ln\delta_s)\right\} + \mathcal{I}_{12}^{\rm fin},\\
&\mathcal{I}_{13} = \mathcal{I}_{24}\\
&\quad = \frac{1}{t_1}\left\{-\frac{1}{\epsilon_{\rm IR}^2} + \frac{1}{\epsilon_{\rm IR}}\left(2\ln\frac{-t_1}{s} + \ln\frac{s}{m_t^2} + 2\ln\delta_s\right)\right\} + \mathcal{I}_{13}^{\rm fin},\\
&\mathcal{I}_{14} = \mathcal{I}_{23}\\
&\quad = \frac{1}{u_1}\left\{-\frac{1}{\epsilon_{\rm IR}^2} + \frac{1}{\epsilon_{\rm IR}}\left(2\ln\frac{-u_1}{s} + \ln\frac{s}{m_t^2} + 2\ln\delta_s\right)\right\} + \mathcal{I}_{14}^{\rm fin},
\end{aligned} \tag{30}$$

where all the IR singularities in $\mathcal{I}_{ij}$ have been extracted out and for briefness, the finite terms $\mathcal{I}_{ij}^{\rm fin}$ are not shown here. Now, Eq. (25) can be rewritten as

$$\begin{aligned}
d\hat{\sigma}^S = &\frac{\alpha_s}{2\pi}C_\epsilon\left[\frac{(A_2^S)_{\rm INT}}{\epsilon_{\rm IR}^2} + \frac{(A_1^S)_{\rm int}}{\epsilon_{\rm IR}} + (A_0^S)_{\rm INT}\right]d\hat{\sigma}_{\rm INT}^{\rm LO}\\
&+ \frac{\alpha_s}{2\pi}C_\epsilon\left[\frac{(A_2^S)_{\rm NPS}}{\epsilon_{\rm IR}^2} + \frac{(A_1^S)_{\rm NPS}}{\epsilon_{\rm IR}} + (A_0^S)_{\rm NPS}\right]d\hat{\sigma}_{\rm NPS}^{\rm LO},
\end{aligned} \tag{31}$$

in which

$$\begin{aligned}
&(A_2^S)_{\rm INT} = 2C_F,\\
&(A_1^S)_{\rm INT} = -\frac{1}{C_A}\left[16\ln\frac{-t_1}{\mu_r^2} + 2\ln\frac{-u_1}{\mu_r^2} + 9\ln\frac{\mu_r^2}{m_t^2}\right.\\
&\qquad\left. + \ln\frac{\mu_r^2}{s} + 16\ln\delta_s - \frac{(1+\beta^2)}{2\beta}\ln\frac{1+\beta}{1-\beta} - 8\right],
\end{aligned} \tag{32}$$

and

$$\begin{aligned}
&(A_2^S)_{\rm NPS} = 2C_F,\\
&(A_1^S)_{\rm NPS} = -2C_F\left[2\ln\frac{-t_1}{\mu_r^2} + \ln\frac{\mu_r^2}{m_t^2} + 2\ln\delta_s - 1\right].
\end{aligned} \tag{33}$$

In the hard collinear region, $E_5 > \delta_s\sqrt{s_{12}}/2$ and $|t_{i5}| < \delta_c s_{12}$, the emitted hard gluon is collinear to one of the incoming partons and the three-body cross section is factorized as

$$\begin{aligned}
d\sigma^{HC} = &\, d\sigma^{\rm LO}\left[\frac{\alpha_s}{2\pi}C_\epsilon'\right]\left(-\frac{1}{\epsilon}\right)\delta_c^{-\epsilon}[P_{dd}(z,\epsilon)\\
&\times G_{d/p}(x_1/z)G_{\bar{d}/p}(x_2) + P_{\bar{d}\bar{d}}(z,\epsilon)G_{\bar{d}/p}(x_1/z)\\
&\times G_{d/p}(x_2) + (x_1 \leftrightarrow x_2)]\frac{dz}{z}\left(\frac{1-z}{z}\right)^{-\epsilon}dx_1dx_2,
\end{aligned} \tag{34}$$

where P_{ij} are the unregulated splitting functions in $n = 4 - 2\epsilon$ dimension for $0 < z < 1$, which is related to the usual Altarelli-Parisi splitting kernels [88] as $P_{ij}(z,\epsilon) = P_{ij}(z) + \epsilon P_{ij}'(z)$. Explicitly, in our case,

$$P_{dd}(z) = P_{\bar{d}\bar{d}}(z) = C_F\frac{1+z^2}{1-z}, \tag{35}$$

$$P_{dd}'(z) = P_{\bar{d}\bar{d}}'(z) = -C_F(1-z). \tag{36}$$

For massless $d(\bar{d})$ emission, we decompose the phase space into two regions, collinear and noncollinear, and give the expression for $gd \to t\bar{t}d$ cross section,

$$\begin{aligned}
d\sigma(qg \to t\bar{t}q) = &\sum_{\alpha=d,\bar{d}}\hat{\sigma}^{\bar{C}}(\alpha g \to t\bar{t}\alpha)[G_{\alpha/p}(x_1)\\
&\times G_{g/p}(x_2) + (x_1 \leftrightarrow x_2)]dx_1dx_2\\
&+ d\sigma^{\rm LO}\left[\frac{\alpha_s}{2\pi}C_\epsilon'\right]\left(-\frac{1}{\epsilon}\right)\delta_c^{-\epsilon}[P_{dg}(z,\epsilon)\\
&\times G_{g/p}(x_1/z)G_{\bar{d}/p}(x_2)\\
&+ P_{\bar{d}g}(z,\epsilon)G_{g/p}(x_1/z)G_{d/p}(x_2)\\
&+ (x_1 \leftrightarrow x_2)]\frac{dz}{z}\left(\frac{1-z}{z}\right)^{-\epsilon}dx_1dx_2,
\end{aligned} \tag{37}$$

where

$$\begin{aligned}
&P_{dg}(z) = P_{\bar{d}g}(z) = \tfrac{1}{2}[z^2 + (1-z)^2],\\
&P_{dg}'(z) = P_{\bar{d}g}'(z) = -z(1-z),
\end{aligned} \tag{38}$$

and

$$\hat{\sigma}^{\bar{C}}(\alpha g \to t\bar{t}\alpha) = \frac{1}{2s_{12}}\int|\mathcal{M}_3|^2(\alpha g \to t\bar{t}\alpha)d\Gamma_3|_{H\bar{C}}. \tag{39}$$

In order to factorize the collinear singularity into the PDF, we introduce a scale dependent PDF in the $\overline{\rm MS}$ convention [84],

$$\begin{aligned}
G_{\alpha/p}(x,\mu_f) = &\, G_{\alpha/p}(x) + \sum_\beta\left(-\frac{1}{\epsilon}\right)\left[\frac{\alpha_s}{2\pi}\left(\frac{4\pi\mu_f^2}{\mu_r^2}\right)^\epsilon\right]\\
&\times\int_x^1\frac{dz}{z}P_{\alpha\beta}(z)G_{\beta/p}(x/z).
\end{aligned} \tag{40}$$

As in Ref. [84], the $\mathcal{O}(\alpha_s)$ collinear contribution is

$$d\sigma^{\rm coll} = d\hat{\sigma}^{\rm LO}\left[\frac{\alpha_s}{2\pi}C'_\epsilon\right]\Big\{\tilde{G}_{d/p}(x_1,\mu_f)G_{\bar{d}/p}(x_2,\mu_f) + G_{d/p}(x_1,\mu_f)\tilde{G}_{\bar{d}/p}(x_2,\mu_f) + \sum_{\alpha=d,\bar{d}}\left[\frac{A_1^{sc}(\alpha\to\alpha g)}{\epsilon} + A_0^{sc}(\alpha\to\alpha g)\right] \times G_{d/p}(x_1,\mu_f)G_{\bar{d}/p}(x_2,\mu_f) + (x_1\leftrightarrow x_2)\Big\}dx_1dx_2, \tag{41}$$

where

$$A_1^{sc}(d\to dg) = A_1^{sc}(\bar{d}\to\bar{d}g) = C_F(2\delta_s + 3/2), \quad A_0^{sc} = A_1^{sc}\ln\frac{s_{12}}{\mu_f^2}, \tag{42}$$

and

$$G_{\alpha/p}(x_1,\mu_f) = \sum_\beta\int_x^{1-\delta s\delta\alpha\beta}\frac{dy}{y}G_{\beta/p}(x_1,\mu_f)\tilde{P}_{\alpha\beta}(y), \tag{43}$$

with

$$\tilde{P}_{\alpha\beta}(y) = P_{\alpha\beta}(y)\ln\left(\delta c\frac{1-y}{y}\frac{s_{12}}{\mu_f^2}\right) - P'_{\alpha\beta}(y). \tag{44}$$

Finally the NLO correction of the $d\bar{d}\to t\bar{t}$ process can be written as

$$\sigma^{\rm NLO} = \int\{dx_1dx_2[G_{d/p}(x_1,\mu_f)G_{\bar{d}/p}(x_2,\mu_f) + (x_1\leftrightarrow x_2)](\sigma^{\rm virt} + \sigma^S + \sigma^{H\bar{C}}) + \sigma^{\rm coll}\} + \sum_{\alpha=d,\bar{d}}\int dx_1dx_2[G_{g/p}(x_1,\mu_f)G_{\alpha/p}(x_2,\mu_f) + (x_1\leftrightarrow x_2)]\sigma^{\bar{C}}(g\alpha\to t\bar{t}\alpha). \tag{45}$$

Note that all the IR divergences in the NLO total cross section are proportional to the LO cross sections. and we find the following relations:

$$\begin{aligned}&(A_2^v)_{\rm INT} + (A_2^S)_{\rm INT} = 0,\\ &(A_1^v)_{\rm INT} + (A_1^S)_{\rm INT} + \sum_{\alpha=d,\bar{d}}A_1^{sc}(\alpha\to\alpha g) = 0,\\ &(A_2^v)_{\rm NPS} + (A_2^S)_{\rm NPS} = 0,\\ &(A_1^v)_{\rm NPS} + (A_1^S)_{\rm NPS} + \sum_{\alpha=d,\bar{d}}A_1^{sc}(\alpha\to\alpha g) = 0.\end{aligned} \tag{46}$$

Now all the IR divergences are canceled exactly.

IV. NUMERICAL RESULTS

In the numerical calculations, we set $m_{W'} = 400$ GeV, because such a W' is readily observed at the Tevatron with an integrated luminosity of 10 fb^{-1}, and at the LHC with an integrated luminosity of 100 pb^{-1} [32]. There are two independent parameters in the NP Lagrangian. For the convenience of calculations we define the parameter set (C_V, C_A), where $C_V = g'(f_R + f_L)/2$ and $C_A = g'(f_R - f_L)/2$. The mass of the top quark is chosen to be $m_t = 172.5$ GeV. The CTEQ6L1 and CTEQ6M PDF sets [89] and the associated α_s functions are used for LO and NLO calculation, respectively. Both the renormalization and factorization scales are fixed to the top quark mass unless specified otherwise.

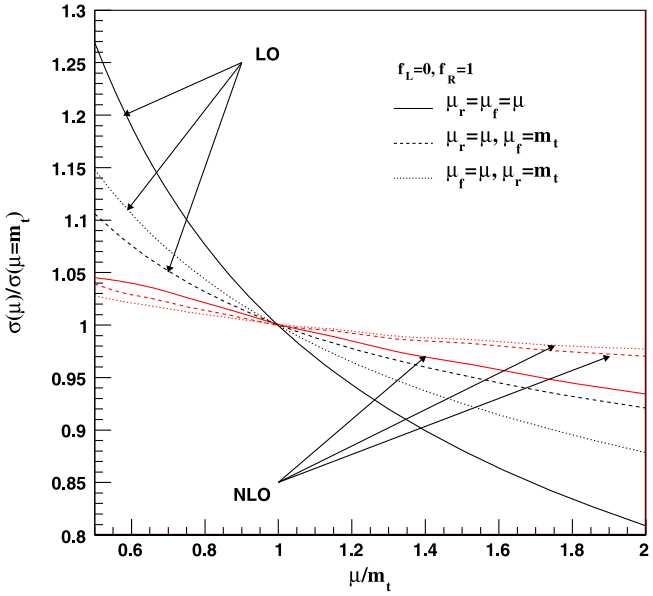

FIG. 6 (color online). Scale dependences of the total cross sections at the Tevatron. The black and the red lines represent the LO and NLO results, respectively.

A. scale dependence

In Fig. 6 we show the scale dependence of the LO and NLO total cross sections at the Tevatron for three cases: (1) the renormalization scale dependence $\mu_r = \mu$, $\mu_f = m_t$; (2) the factorization scale dependence $\mu_r = m_t$, $\mu_f = \mu$; and (3) the total scale dependence $\mu_r = \mu_f = \mu$. From Fig. 6, we can see that the NLO corrections significantly reduce the scale dependence for all three cases, making the theoretical predictions more reliable.

B. Tevatron constraints

$A_{\rm FB}$ of top quark pair productions is defined as

$$A_{\rm FB} = \frac{\sigma_{\rm F} - \sigma_{\rm B}}{\sigma_{\rm F} + \sigma_{\rm B}} = A_{\rm FB}^{\rm NP}\times R + A_{\rm FB}^{\rm SM}\times(1-R),$$

where

$$A_{\rm FB}^{\rm NP} = (\sigma_{\rm F}^{\rm NP} - \sigma_{\rm B}^{\rm NP})/(\sigma_{\rm F}^{\rm NP} + \sigma_{\rm B}^{\rm NP}),$$
$$A_{\rm FB}^{\rm SM} = (\sigma_{\rm F}^{\rm SM} - \sigma_{\rm B}^{\rm SM})/(\sigma_{\rm F}^{\rm SM} + \sigma_{\rm B}^{\rm SM}),$$
$$R = \sigma_{\rm tot}^{\rm NP}/(\sigma_{\rm tot}^{\rm SM} + \sigma_{\rm tot}^{\rm NP}) \quad (47)$$

are the asymmetries induced by NP and SM, and R is the fraction of the NP contribution to the total cross section. $\sigma_{\rm F}$ and $\sigma_{\rm B}$ denote the total cross sections in the forward (F) and backward (B) rapidity regions, respectively. The LO and NLO total cross sections of the interference and NP contributions can be written in terms of C_V^2 and C_A^2,

$$[\sigma_{t\bar{t}}^{\rm INT}]_{\rm LO} = [-1.28^{+0.36}_{-0.25}(C_V^2 + C_A^2)]\ {\rm pb}, \quad (48)$$

$$[\sigma_{t\bar{t}}^{\rm NPS}]_{\rm LO} = [2.15^{+0.35}_{-0.28}(C_V^2 + C_A^2)^2 - 2.61^{+0.41}_{-0.34}(C_V^2 \cdot C_A^2)]\ {\rm pb}, \quad (49)$$

and

$$[\sigma_{t\bar{t}}^{\rm INT}]_{\rm NLO} = [-1.56^{+0.11}_{-0.13}(C_V^2 + C_A^2)]\ {\rm pb}, \quad (50)$$

$$[\sigma_{t\bar{t}}^{\rm NPS}]_{\rm NLO} = [2.48^{+0.07}_{-0.12}(C_V^2 + C_A^2)^2 - 2.92^{+0.06}_{-0.12}(C_V^2 \cdot C_A^2)]\ {\rm pb}, \quad (51)$$

where the errors are obtained by varying the scale between $\mu_r = \mu_f = m_t/2$ and $\mu_r = \mu_f = 2m_t$. The differences of the cross sections in the forward and backward rapidity region are given by

$$[\sigma_{\rm F}^{\rm INT} - \sigma_{\rm B}^{\rm INT}]_{\rm LO} = [-0.31^{-0.07}_{+0.10}(C_V^2 + C_A^2)]\ {\rm pb}, \quad (52)$$

$$[\sigma_{\rm F}^{\rm NPS} - \sigma_{\rm B}^{\rm NPS}]_{\rm LO} = [0.73^{-0.11}_{+0.13}(C_V^2 + C_A^2)^2 + 0.050^{-0.003}_{+0.011}(C_V^2 \cdot C_A^2)]\ {\rm pb}, \quad (53)$$

and

$$[\sigma_{\rm F}^{\rm INT} - \sigma_{\rm B}^{\rm INT}]_{\rm NLO} = [-0.44^{-0.05}_{+0.04}(C_V^2 + C_A^2)]\ {\rm pb}, \quad (54)$$

$$[\sigma_{\rm F}^{\rm NPS} - \sigma_{\rm B}^{\rm NPS}]_{\rm NLO} = [0.99^{-0.03}_{+0.04}(C_V^2 + C_A^2)^2 - 0.130^{-0.002}_{+0.002}(C_V^2 \cdot C_A^2)]\ {\rm pb}. \quad (55)$$

For the $t\bar{t}$ invariant mass spectrum, we restrict our attention to the large invariant mass region, i.e. $m_{t\bar{t}} \in [800, 1400]$ GeV, where the $A_{\rm FB}$ is the most obvious. The results are presented as

$$\left[\frac{d\sigma_{t\bar{t}}^{\rm INT}}{dm_{t\bar{t}}}\right]_{\rm LO}^{m_{t\bar{t}}\in[800,1400]} = [-0.019^{+0.008}_{-0.005}(C_V^2 + C_A^2)]\frac{\rm pb}{\rm GeV}, \quad (56)$$

$$\left[\frac{d\sigma_{t\bar{t}}^{\rm NPS}}{dm_{t\bar{t}}}\right]_{\rm LO}^{m_{t\bar{t}}\in[800,1400]} = [0.101^{+0.018}_{-0.021}(C_V^2 + C_A^2)^2 - 0.086^{+0.015}_{-0.020}(C_V^2 \cdot C_A^2)]\frac{\rm pb}{\rm GeV}, \quad (57)$$

and

$$\left[\frac{d\sigma_{t\bar{t}}^{\rm INT}}{dm_{t\bar{t}}}\right]_{\rm NLO}^{m_{t\bar{t}}\in[800,1400]} = [-0.026^{+0.004}_{-0.002}(C_V^2 + C_A^2)]\frac{\rm pb}{\rm GeV}, \quad (58)$$

$$\left[\frac{d\sigma_{t\bar{t}}^{\rm NPS}}{dm_{t\bar{t}}}\right]_{\rm NLO}^{m_{t\bar{t}}\in[800,1400]} = [0.125^{+0.040}_{-0.018}(C_V^2 + C_A^2)^2 - 0.010^{+0.007}_{-0.008}(C_V^2 \cdot C_A^2)]\frac{\rm pb}{\rm GeV}. \quad (59)$$

From the errors in Eqs. (48)–(59) we can see that NLO corrections reduce the dependence of the cross sections on the renormalization and factorization scales.

In Fig. 7, we show the allowed region in the (C_V, C_A) plane that is consistent with the total cross section $\sigma_{t\bar{t}}$, $A_{\rm FB}$ [9] and the spectrum of $m_{t\bar{t}}$ in the large mass region [90], which are given by

$$\sigma_{t\bar{t}}^{\rm EX} = (7.50 \pm 0.48)\ {\rm pb}, \quad (60)$$

$$A_{\rm FB}^{\rm EX} = 0.475 \pm 0.114, \quad \text{for } m_{t\bar{t}} > 450\ {\rm GeV}, \quad (61)$$

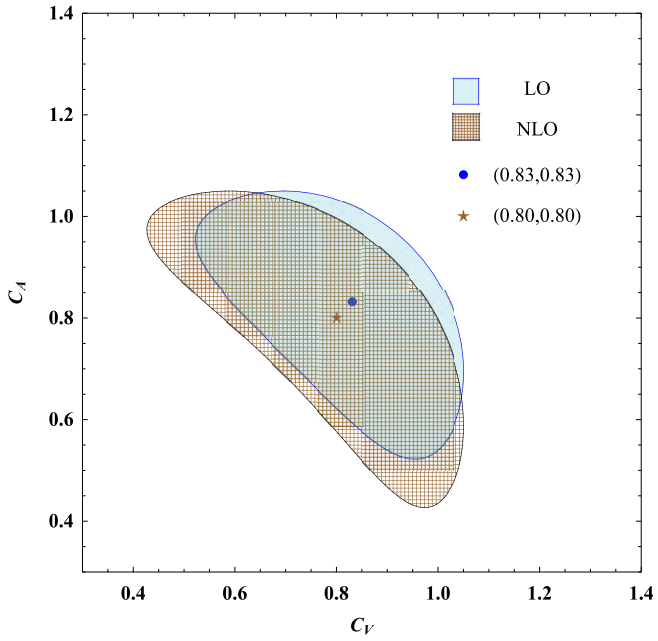

FIG. 7 (color online). Values of C_V and C_A allowed by Tevatron data at 95% C.L.: $\sigma_{t\bar{t}} = (7.50 \pm 0.48)$ pb, $A_{\rm FB}(m_{t\bar{t}} > 450\ {\rm GeV}) = 0.475 \pm 0.114$, and $(d\sigma_{t\bar{t}}/dm_{t\bar{t}})^{m_{t\bar{t}}\in[800,1400]\ {\rm GeV}} = (0.068 \pm 0.036)$ fb/GeV. The blue dot (0.83, 0.83) and brown star (0.80, 0.80) represent the BFPs at LO and NLO levels, respectively. The allowed parameter region is symmetric with respect to the C_A and C_V axes, so we only display the contours where C_A and $C_V > 0$.

$$\left[\frac{d\sigma_{t\bar{t}}}{dm_{t\bar{t}}}\right]^{m_{t\bar{t}}\in[800,1400]\ \mathrm{GeV}}_{\mathrm{EX}} = (0.068 \pm 0.036)\ \mathrm{fb/GeV}. \tag{62}$$

We use Monte Carlo program MCFM [91] to get the cross section of the gluon fusion channel $gg \to t\bar{t}$ and quark channel $q\bar{q} \to t\bar{t}$ at the NLO QCD level. Combining the contributions of these two channels we have the SM predictions for the above observables at the NLO level

$$\sigma^{\mathrm{SM}}_{t\bar{t}} = 7.00^{+0.36}_{-0.76}\ \mathrm{pb}, \tag{63}$$

$$\left[\frac{d\sigma_{t\bar{t}}}{dm_{t\bar{t}}}\right]^{m_{t\bar{t}}\in[800,1400]\ \mathrm{GeV}}_{\mathrm{SM}} = 0.055^{+0.010}_{-0.005}\ \mathrm{fb/GeV}, \tag{64}$$

where we have considered scale uncertainty in the calculations. We have used the SM QCD predicted values of $A_{\mathrm{FB}}(m_{t\bar{t}} \geq 450\ \mathrm{GeV}) = 0.088 \pm 0.013$ at the NLO level, although next-to-next-to-leading logarithmic (NNLL) SM QCD results are available [6].

The measurements of A_{FB} and invariant mass spectrum $d\sigma_{t\bar{t}}/dm_{t\bar{t}}$ in the large invariant mass region are particularly sensitive to values of C_V and C_A at the NLO level. In order to generate the desired A_{FB} in the large $m_{t\bar{t}}$ region, NP couplings should be large enough so that the positive NPS terms could overcome the negative INT terms. While on the other hand, the NLO NPS effect causes the cross section in the last bin of $m_{t\bar{t}}$ to exceed the 1σ upper limit of the experimental result and therefore we expect the couplings C_V and C_A to not be too large. As a consequence, NP couplings are subject to strong restrictions.

In Fig. 7, the solid and grid regions correspond to NP LO and NLO results at 95% confidence level (C.L.), where we have considered theoretical and experimental uncertainty in $\sigma_{t\bar{t}}$ and $d\sigma_{t\bar{t}}/m_{t\bar{t}}$ and only consider experimental uncertainty in the calculation of A_{FB}. It can be seen that NLO corrections manifestly changed the allowed parameter region of C_V and C_A. The blue dot (0.83, 0.83) and brown star (0.80, 0.80) represent the best fit points (BFPs) at the LO and NLO levels, where χ^2 reaches its minimums of 2.1 and 1.8, respectively. Thus we can see that higher order corrections loosen the restrictions on NP couplings and reduce the BFPs of C_V and C_A by 3%.

Now we discuss the theoretical predictions for the measurements at Tevatron induced by NP at the NLO BFP (0.80, 0.80), or equivalently, $g' = 1.48$, and $f_R = 1$, $f_L = 0$: The LO and NLO total cross sections of $t\bar{t}$ production are

$$\sigma^{\mathrm{NP}}_{t\bar{t},\mathrm{LO}} = 0.813\ \mathrm{pb}, \qquad \sigma^{\mathrm{NP}}_{t\bar{t},\mathrm{NLO}} = 0.867\ \mathrm{pb}, \tag{65}$$

and the differential cross sections are

$$\begin{aligned}[d\sigma^{\mathrm{NP}}_{t\bar{t}}/dm_{t\bar{t}}]^{m_{t\bar{t}}\in[800,1400]\mathrm{GeV}}_{\mathrm{LO}} &= 0.105\ \mathrm{fb/GeV},\\ [d\sigma^{\mathrm{NP}}_{t\bar{t}}/dm_{t\bar{t}}]^{m_{t\bar{t}}\in[800,1400]\mathrm{GeV}}_{\mathrm{NLO}} &= 0.130\ \mathrm{fb/GeV}.\end{aligned} \tag{66}$$

Here, the superscript NP represents the combination of the INT and NPS contributions mentioned above. It can be seen that the NLO corrections have slight effects on the total cross section but increase the invariant mass distribution in the large mass region. Note that the two parts of the NP corrections, INT and NPS terms, are individually not small, but they have opposite sign and cancel each other.

The A_{FB} containing NP contributions at the NLO BFP are shown in Table I. All the theoretical predictions containing NP NLO effects are consistent with experimental results within 2σ C.L. It is found that the A_{FB} in the large invariant mass region gets an obvious enhancement by about 9%.

In Fig. 8, we show differential cross section $d\sigma/dm_{t\bar{t}}$ when we consider NP effects at the NLO BFP, from which we can see that higher order corrections do not change the distribution very much.

In the above discussions on top quark asymmetries in the production at the Tevatron, we have only calculated partonic differential cross sections. But in the experiments there are several cuts imposed on the decay products of the (anti)top quark so that our results can be meaningful only if the effects of the NP do not change the kinematic distributions of the top quark pairs much. To illustrate this point, we show the p_T and η distributions of the top quark with and without NP effects in Fig. 9. Here we take into account only the LO NP effects for comparison since including the NLO correction will not obviously change the distributions. We can see that the p_T distribution is enhanced by the NP effects in general while the η distribution only in the forward region is increased. The fact that the shapes of the two distributions have not changed a lot after including the NP effects makes us believe that the A_{FB} we have calculated can be compared with the experimental values.

TABLE I. The A_{FB} with $g' = 1.48$, $f_R = 1$, $f_L = 0$, and $M_{W'} = 400$ GeV at the Tevatron, where $A^{p\bar{p}}_{\mathrm{FB}}$ and $A^{t\bar{t}}_{\mathrm{FB}}$ are the A_{FB} in the lab frame and the $t\bar{t}$ rest frame, respectively. Here we list the C.L. when including NP effects at the NLO level.

	SM NLO QCD + NP LO	SM NLO QCD + NP NLO
$A^{p\bar{p}}_{\mathrm{FB}}$	0.179	0.197 (0.1σ)
$A^{t\bar{t}}_{\mathrm{FB}}$	0.185	0.202 (0.6σ)
$A^{t\bar{t}}_{\mathrm{FB}}(m_{t\bar{t}} < 450\ \mathrm{GeV})$	0.062	0.063 (1.2σ)
$A^{t\bar{t}}_{\mathrm{FB}}(m_{t\bar{t}} > 450\ \mathrm{GeV})$	0.313	0.343 (1.2σ)

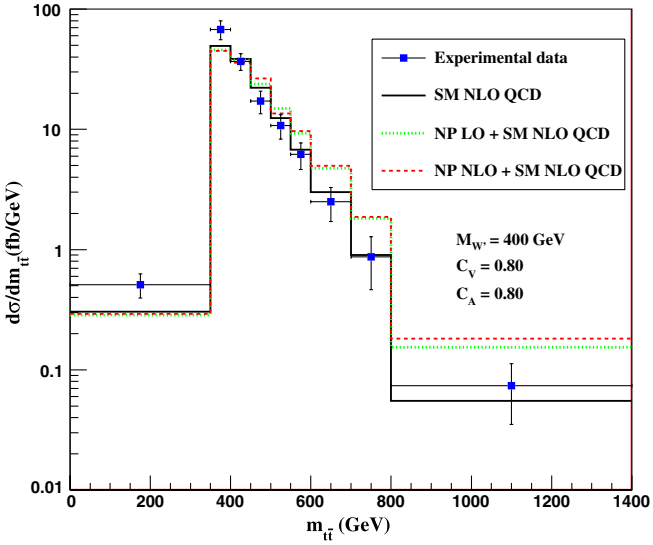

FIG. 8 (color online). Differential cross sections $d\sigma/dm_{t\bar{t}}$ as a function of $m_{t\bar{t}}$ at the NLO BFPs $(\pm 0.80, \pm 0.80)$. Here "Experimental data" are $d\sigma/dm_{t\bar{t}}$ measured with 2.7 fb^{-1} of integrated luminosity at the Tevatron [90]. "SM NLO QCD" represents the results in the SM QCD at the NLO level. "NP LO + SM NLO QCD" and "NP NLO + SM NLO QCD" stand for the predictions including NP effects at LO and NLO levels, respectively.

C. LHC predictions

The process of top quark pair production has been measured at the LHC, and the cross section [92,93] is

$$\sigma_{t\bar{t}}^{\mathrm{ATLAS}}(\mathrm{LHC}, \sqrt{S} = 7\ \mathrm{TeV}) = 180 \pm 18\ \mathrm{pb}, \quad (67)$$

$$\sigma_{t\bar{t}}^{\mathrm{CMS}}(\mathrm{LHC}, \sqrt{S} = 7\ \mathrm{TeV}) = 158 \pm 19\ \mathrm{pb}, \quad (68)$$

which are consistent with the SM predictions. Since the LHC is a proton-proton collider, which is forward-backward symmetric, the A_{FB} defined at the Tevatron cannot be directly applied to the proton-proton collider experiments at the LHC. A_C used by CMS [94,95] is defined as

$$A_C = \frac{\sigma(|\eta_t| - |\eta_{\bar{t}}| > 0) - \sigma(|\eta_t| - |\eta_{\bar{t}}| < 0)}{\sigma(|\eta_t| - |\eta_{\bar{t}}| > 0) + \sigma(|\eta_t| - |\eta_{\bar{t}}| < 0)}, \quad (69)$$

where η_t and $\eta_{\bar{t}}$ are pseudorapidities of the top and antitop quarks, respectively. Last year at CMS, it is measured to be [94]

$$A_C = 0.060 \pm 0.134(\mathrm{stat}) \pm 0.026(\mathrm{syst}),$$

whereas the recently updated report shows [95]

$$A_C = -0.016 \pm 0.030(\mathrm{stat}) \pm 0.019(\mathrm{syst}).$$

The discrepancy between these two measurements is evident. However, given the large experimental error, both results are compatible with the SM predictions $A_C = 0.013$ [94]. The A_C induced by NP interactions at the NP NLO BFPs $(\pm 0.80, \pm 0.80)$ is 0.081, which is about 6 times that of the SM prediction. This result is close to the observed central value at CMS [94], and is also consistent with the latest data value [95] within 2σ C.L. We still need more experimental data with higher precision to seek evidence for a possible modification in A_C by NP.

In Fig. 10, we show the results of a combined fit to the $t\bar{t}$ data in the presence of NP at a different C.L. The shadows from dark to light indicate the experimentally preferred regions of 95%, 97%, and 99% probability in the $C_V - C_A$ plane. The black dot represents the SM point (0,0), and the black star represents the NLO BFP (C_V, C_A). At the LHC with $\sqrt{S} = 7$ TeV, the cross section of $t\bar{t}$ production at the NLO QCD level in the SM is $\sigma_{t\bar{t}} = 154.5$ pb. Including NP contributions at the NLO BFP, we have $\sigma_{t\bar{t},\mathrm{NLO}}^{\mathrm{NP+SM}} = 184$ pb.

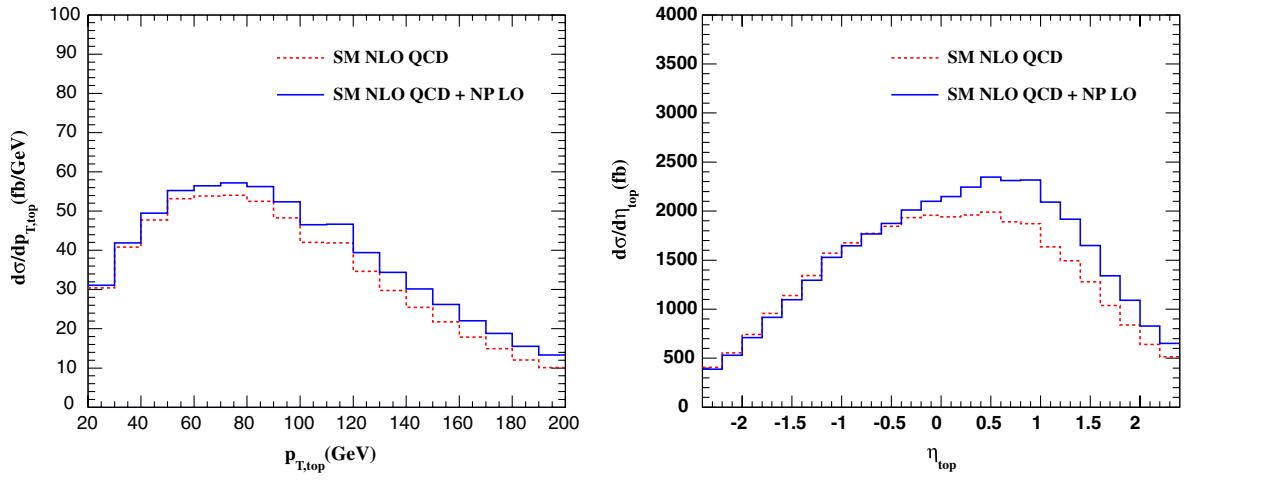

FIG. 9 (color online). The p_T (left panel) and η (right panel) distributions of the top quark at the Tevatron. The red dashed lines denote the contributions of the SM at the NLO QCD level while the blue solid lines include NP effects at LO in addition.

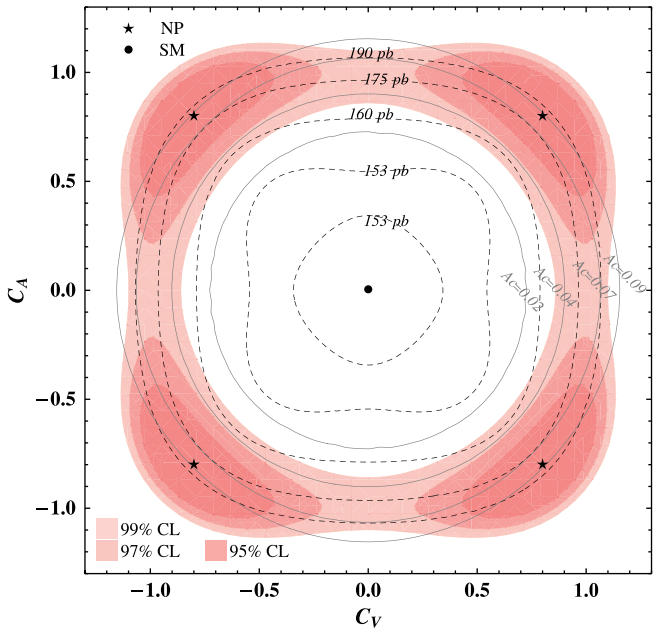

FIG. 10 (color online). Results of a combined fit to $\sigma_{t\bar{t}}$ and the value of A_{FB} allowing for NP at different C.L.s. The shadows from dark to light indicate the experimentally favored regions of 95%, 97%, and 99% probability in the $C_V - C_A$ plane. The black dashed lines and gray solid lines, respectively, represent the value of the total $t\bar{t}$ cross section and the A_C at the LHC with $\sqrt{S} = 7$ TeV. The black dot and stars represent the SM point and the NP NLO BFPs.

From the shape of contours of $\sigma_{t\bar{t}}$ and A_C, one may easily distinguish NP events from SM ones. The location of the brown contours indicates that vector current C_V or axial currrent C_A alone cannot improve the quality of fit significantly. The acceptable confidence region (global 95% C.L.) centers around four points in the parameter space where $|C_V|$ equals $|C_A|$, which means experimental data favor purely right-handed or left-handed couplings.

V. CONCLUSION

We have investigated the NLO QCD effect on the total cross section, invariant mass distribution, and forward-backward asymmetry A_{FB} of top quark pair production mediated by W' at the Tevatron and the LHC. We have taken into account the interference of the NP channel with QCD channel [up to $\mathcal{O}(\alpha_s^2 g'^2)$], as well as the interference between NP channels [up to $\mathcal{O}(\alpha_s g'^4)$]. We fit the data at the Tevatron, including total cross section, the invariant mass distribution, and the A_{FB}, and find the allowed parameter space. We show that at our BFP, due to the cancellation between these two parts of contributions, the NLO total cross section exhibits only a slight modification compared to the LO result of NP. But the A_{FB} is increased by about 9%. As a result, after NLO contributions are taken into account, it is more likely to simultaneously satisfy the constraints from the data of A_{FB} and the $d\sigma/dm_{t\bar{t}}$ spectrum in the large invariant mass region at the Tevatron. At the LHC, both total cross section and A_C can be used to distinguish NP from the SM and therefore the LHC may detect these NP effects with the integrated luminosity increasing.

ACKNOWLEDGMENTS

This work was supported by the Undergraduate Research Fund of the Education Foundation of Peking University and the National Natural Science Foundation of China, under Grants No. 11021092 and No. 10975004.

[1] J. H. Kuhn and G. Rodrigo, Phys. Rev. Lett. **81**, 49 (1998).
[2] J. H. Kuhn and G. Rodrigo, Phys. Rev. D **59**, 054017 (1999).
[3] M. T. Bowen, S. D. Ellis, and D. Rainwater, Phys. Rev. D **73**, 014008 (2006).
[4] L. G. Almeida, G. F. Sterman, and W. Vogelsang, Phys. Rev. D **78**, 014008 (2008).
[5] O. Antunano, J. H. Kuhn, and G. Rodrigo, Phys. Rev. D **77**, 014003 (2008).
[6] V. Ahrens, A. Ferroglia, M. Neubert, B. D. Pecjak, and L. L. Yang, Phys. Rev. D **84**, 074004 (2011).
[7] V. M. Abazov *et al.* (D0 Collaboration), Phys. Rev. Lett. **100**, 142002 (2008).
[8] T. Aaltonen *et al.* (CDF Collaboration), Phys. Rev. Lett. **101**, 202001 (2008).
[9] T. Aaltonen *et al.* (CDF Collaboration), Phys. Rev. D **83**, 112003 (2011).
[10] Y.-C. Chen, arXiv:1107.0239.
[11] A. Djouadi, G. Moreau, F. Richard, and R. K. Singh, Phys. Rev. D **82**, 071702 (2010).
[12] S. Jung, H. Murayama, A. Pierce, and J. D. Wells, Phys. Rev. D **81**, 015004 (2010).
[13] K. Cheung, W.-Y. Keung, and T.-C. Yuan, Phys. Lett. B **682**, 287 (2009).
[14] P. H. Frampton, J. Shu, and K. Wang, Phys. Lett. B **683**, 294 (2010).
[15] J. Shu, T. M. P. Tait, and K. Wang, Phys. Rev. D **81**, 034012 (2010).
[16] A. Arhrib, R. Benbrik, and C.-H. Chen, Phys. Rev. D **82**, 034034 (2010).
[17] P. Ferrario and G. Rodrigo, J. High Energy Phys. 02 (2010) 051.
[18] I. Dorsner, S. Fajfer, J. F. Kamenik, and N. Kosnik, Phys. Rev. D **81**, 055009 (2010).
[19] D.-W. Jung, P. Ko, J. S. Lee, and S.-h. Nam, Phys. Lett. B **691**, 238 (2010).

[20] J. Cao, Z. Heng, L. Wu, and J. M. Yang, Phys. Rev. D **81**, 014016 (2010).
[21] V. Barger, W.-Y. Keung, and C.-T. Yu, Phys. Rev. D **81**, 113009 (2010).
[22] Q.-H. Cao, D. McKeen, J. L. Rosner, G. Shaughnessy, and C. E. M. Wagner, Phys. Rev. D **81**, 114004 (2010).
[23] B. Xiao, Y.-k. Wang, and S.-h. Zhu, Phys. Rev. D **82**, 034026 (2010).
[24] M. V. Martynov and A. D. Smirnov, Mod. Phys. Lett. A **25**, 2637 (2010).
[25] R. S. Chivukula, E. H. Simmons, and C. P. Yuan, Phys. Rev. D **82**, 094009 (2010).
[26] M. Bauer, F. Goertz, U. Haisch, T. Pfoh, and S. Westhoff, J. High Energy Phys. 11 (2010) 039.
[27] C.-H. Chen, G. Cvetic, and C. S. Kim, Phys. Lett. B **694**, 393 (2011).
[28] D.-W. Jung, P. Ko, and J. S. Lee, Phys. Lett. B **701**, 248 (2011).
[29] G. Burdman, L. de Lima, and R. D. Matheus, Phys. Rev. D **83**, 035012 (2011).
[30] D.-w. Jung, P. Ko, J. S. Lee, and S.-h. Nam, Proc. Sci. ICHEP2010 (2010) 397.
[31] D. Choudhury, R. M. Godbole, S. D. Rindani, and P. Saha, Phys. Rev. D **84**, 014023 (2011).
[32] K. Cheung and T.-C. Yuan, Phys. Rev. D **83**, 074006 (2011).
[33] J. Cao, L. Wang, L. Wu, and J. M. Yang, Phys. Rev. D **84**, 074001 (2011).
[34] E. L. Berger, Q.-H. Cao, C.-R. Chen, C. S. Li, and H. Zhang, Phys. Rev. Lett. **106**, 201801 (2011).
[35] V. Barger, W.-Y. Keung, and C.-T. Yu, Phys. Lett. B **698**, 243 (2011).
[36] B. Bhattacherjee, S. S. Biswal, and D. Ghosh, Phys. Rev. D **83**, 091501 (2011).
[37] K. Blum *et al.*, Phys. Lett. B **702**, 364 (2011).
[38] K. M. Patel and P. Sharma, J. High Energy Phys. 04 (2011) 085.
[39] G. Isidori and J. F. Kamenik, Phys. Lett. B **700**, 145 (2011).
[40] A. R. Zerwekh, Phys. Lett. B **704**, 62 (2011).
[41] E. R. Barreto, Y. A. Coutinho, and J. Sa Borges, Phys. Rev. D **83**, 054006 (2011).
[42] R. Foot, Phys. Rev. D **83**, 114013 (2011).
[43] Z. Ligeti, G. M. Tavares, and M. Schmaltz, J. High Energy Phys. 06 (2011) 109.
[44] M. I. Gresham, I.-W. Kim, and K. M. Zurek, Phys. Rev. D **83**, 114027 (2011).
[45] S. Jung, A. Pierce, and J. D. Wells, Phys. Rev. D **83**, 114039 (2011).
[46] M. R. Buckley, D. Hooper, J. Kopp, and E. T. Neil, Phys. Rev. D **83**, 115013 (2011).
[47] J. Shu, K. Wang, and G. Zhu, arXiv:1104.0083 [Phys. Rev. D (to be published)].
[48] J. A. Aguilar-Saavedra and M. Perez-Victoria, Phys. Lett. B **701**, 93 (2011).
[49] C.-H. Chen, S. S. C. Law, and R.-H. Li, J. Phys. G **38**, 115008 (2011).
[50] C. Degrande, J.-M. Gerard, C. Grojean, F. Maltoni, and G. Servant, Phys. Lett. B **703**, 306 (2011).
[51] S. Jung, A. Pierce, and J. D. Wells, Phys. Rev. D **84**, 055018 (2011).
[52] D.-W. Jung, P. Ko, and J. S. Lee, Phys. Rev. D **84**, 055027 (2011).
[53] K. S. Babu, M. Frank, and S. K. Rai, Phys. Rev. Lett. **107**, 061802 (2011).
[54] A. Djouadi, G. Moreau, and F. Richard, Phys. Lett. B **701**, 458 (2011).
[55] R. Barcelo, A. Carmona, M. Masip, and J. Santiago, Phys. Rev. D **84**, 014024 (2011).
[56] D. Krohn, T. Liu, J. Shelton, and L.-T. Wang, Phys. Rev. D **84**, 074034 (2011).
[57] J. A. Aguilar-Saavedra and M. Perez-Victoria, Phys. Rev. D **84**, 115013 (2011).
[58] Y. Cui, Z. Han, and M. D. Schwartz, J. High Energy Phys. 07 (2011) 127.
[59] A. Hektor *et al.*, Phys. Rev. D **84**, 031701 (2011).
[60] E. Gabrielli and M. Raidal, Phys. Rev. D **84**, 054017 (2011).
[61] M. Duraisamy, A. Rashed, and A. Datta, Phys. Rev. D **84**, 054018 (2011).
[62] J. A. Aguilar-Saavedra and M. Perez-Victoria, J. High Energy Phys. 09 (2011) 097.
[63] R. Barcelo, A. Carmona, M. Masip, and J. Santiago, Phys. Lett. B **707**, 88 (2012).
[64] G. M. Tavares and M. Schmaltz, Phys. Rev. D **84**, 054008 (2011).
[65] L. Vecchi, J. High Energy Phys. 10 (2011) 003.
[66] K. Blum, Y. Hochberg, and Y. Nir, J. High Energy Phys. 10 (2011) 124.
[67] C. Degrande, J.-M. Gerard, C. Grojean, F. Maltoni, and G. Servant, J. High Energy Phys. 03 (2011) 125.
[68] J. A. Aguilar-Saavedra and M. Perez-Victoria, J. High Energy Phys. 05 (2011) 034.
[69] D. Y. Shao *et al.*, Phys. Rev. D **84**, 054016 (2011).
[70] P. Ko, Y. Omura, and C. Yu, arXiv:1108.0350.
[71] M. Frank, A. Hayreter, and I. Turan, Phys. Rev. D **84**, 114007 (2011).
[72] H. Davoudiasl, T. McElmurry, and A. Soni, arXiv:1108.1173.
[73] S. Jung, A. Pierce, and J. D. Wells, Phys. Rev. D **84**, 091502 (2011).
[74] S. Westhoff, arXiv:1108.3341.
[75] G. Z. Krnjaic, Phys. Rev. D **85**, 014030 (2012).
[76] E. L. Berger, arXiv:1109.3202.
[77] J. A. Aguilar-Saavedra, A. Juste, and F. Rubbo, Phys. Lett. B **707**, 92 (2012).
[78] J. Cao, K. Hikasa, L. Wang, L. Wu, and J. M. Yang, arXiv:1109.6543 [Phys. Rev. D (to be published)].
[79] J. H. Kuhn and G. Rodrigo, arXiv:1109.6830 [J. High Energy Phys. (to be published)].
[80] M. Endo and S. Iwamoto, arXiv:1110.0014.
[81] K. Kolodziej, arXiv:1110.2103.
[82] J. Cao, Z. Heng, L. Wu, and J. M. Yang, Phys. Rev. D **81**, 014016 (2010).
[83] B. Xiao, Y.-k. Wang, and S.-h. Zhu, Phys. Rev. D **82**, 034026 (2010).
[84] B. W. Harris and J. F. Owens, Phys. Rev. D **65**, 094032 (2002).
[85] J. Collins, F. Wilczek, and A. Zee, Phys. Rev. D **18**, 242 (1978).
[86] H. X. Zhu *et al.*, J. High Energy Phys. 09 (2011) 043.

[87] G. P. Lepage, J. Comput. Phys. **27**, 192 (1978).
[88] G. Altarelli and G. Parisi, Nucl. Phys. **B126**, 298 (1977).
[89] J. Pumplin *et al.*, J. High Energy Phys. 07 (2002) 012.
[90] T. Aaltonen *et al.* (CDF Collaboration), Phys. Rev. Lett. **102**, 222003 (2009).
[91] J. M. Campbell and R. K. Ellis, Phys. Rev. D **60**, 113006 (1999).
[92] A. Roe, Technical Report No. ATL-PHYS-PROC-2011-178, CERN, Geneva, 2011.
[93] CMS Collaboration, Report No. CMS-PAS-TOP-11-001, 2011.
[94] CMS Collaboration, Report No. CMS-PAS-TOP-10-010, 2011.
[95] CMS Collaboration, Report No. CMS-PAS-TOP-11-014, 2011.